OPEN ACCESS
IOP Publishing | ISECAEP
Journal of Reliability Science and Engineering
J. Reliab. Sci. Eng. **2** (2026) 035302 (15pp)
https://doi.org/10.1088/3050-2454/ae8dd1

Cross-cycle health indicator construction and state of health prediction of lithium-ion batteries by cross recurrence quantification analysis

Le Wang[1], Shuaijie Chen[1], Zhiqiang Cai[2], Weiyan Liu[1,*] and Zhenggeng Ye[1,*]

[1] Department of Industrial Engineering, School of Management, Zhengzhou University, Zhengzhou 450001, People's Republic of China
[2] Department of Industrial Engineering & Ministry of Industry and Information Technology Key Laboratory of Industrial Engineering and Intelligent Manufacturing, Northwestern Polytechnical University, Xi'an 710072, People's Republic of China

E-mail: gllwy@zzu.edu.cn and yezhenggeng@zzu.edu.cn

Received 28 April 2026, revised 29 June 2026
Accepted for publication 20 July 2026
Published 5 August 2026

Abstract

The state of health (SOH) is a key indicator of lithium-ion battery degradation, whose accurate assessment is essential for the reliable operation of battery driven systems. Most existing methods rely on features derived from individual or adjacent cycles, which cannot exploit variation information hidden in monitored signals across different cycles. To address this issue, this paper proposes a novel framework that uses cross-cycle features to estimate the SOH in a derivative manner. Firstly, cross-recurrence quantification analysis (CRQA) is applied to compare battery signals across different cycles, constructing CRQA metric matrix families that reflect cross-cycle variations in raw measurements. Then, the variation of SOH (ΔSOH) between any two cycles is introduced as the prediction target, instead of predicting SOH directly. Next, a convolutional neural network with time series cross-validation is developed to predict ΔSOH, preserving the temporal dependency inherent in ΔSOH. Finally, the proposed framework is implemented and tested on the NASA battery dataset, where the prediction performance is evaluated and compared. The experimental results show a mean absolute error of 0.2965% and a root mean square error of 0.4156%, confirming the feasibility and potential of the cross-cycle health indicator-based indirect approach in battery SOH estimation.

Keywords: lithium-ion battery, state of health, cross-recurrence quantification analysis, prediction, cross-cycle features

* Authors to whom any correspondence should be addressed.

Original content from this work may be used under the terms of the Creative Commons Attribution 4.0 licence. Any further distribution of this work must maintain attribution to the author(s) and the title of the work, journal citation and DOI.

© 2026 The Author(s). Published by IOP Publishing Ltd on behalf of the Institute of Systems Engineering, China Academy of Engineering Physics

1. Introduction

Lithium-ion batteries are widely used in electric vehicles due to their high energy density, but they inevitably degrade with cycling [1]. Battery degradation can increase the risk of short circuits and thermal runaway [2]. The largest proportion of electric vehicle fire accidents occur during the charging process, where excessive heat generation can accelerate degradation and trigger thermal runway [3]. Therefore, accurate reliability assessment of batteries is essential for effective warranty management [4], timely replacement and accident prevention. Reliability science provides the fundamental framework for understanding and assessing the degradation and failure processes of engineering systems [5]. State of health (SOH) is a commonly used indicator that quantifies battery degradation and can guide predictive maintenance and replacement decisions [6].

Data-driven methods, which estimate SOH from monitoring data using algorithms, have been widely adopted as they do not require knowledge of the battery's internal mechanisms [7], in contrast to physics-guided models that rely on electrochemical parameterization. Data-driven SOH prediction typically involves two stages: feature extraction and prediction modeling [8]. During feature extraction, health indicators (HIs) derived from charge-discharge cycle data, including voltage, current, and temperature, are frequently used. Basic features such as constant-current charging time and constant-voltage charging time [9] are widely used. Besides, more advanced features, including voltage change rate from 300s to 1000s [9], the charging duration of equal voltage intervals during constant current charging [10], and point-to-point time integral impedance features derived from charging voltage curves [11], have also been proposed. In addition to raw charge-discharge data, electrochemical features such as IC curve characteristics [12] and internal resistance [13] are also popular. Beyond manually designed features, Liu *et al* [1] proposed the RCMHCRE algorithm to automatically extract HIs directly from raw voltage and current data; Chae and Bae [14] developed an unsupervised Bayesian convolutional autoencoder that automatically extracts latent features from raw signals as virtual HIs. Moreover, various feature selection and fusion strategies have been explored to obtain highly correlated features, such as Pearson correlation, Principal Component Analysis and grey relational analysis [15, 16]. Then, for prediction modeling, common methods include support vector regression (SVR), long short-term memory (LSTM) [16], convolutional neural networks (CNN) [17], etc. To optimize model hyperparameters, techniques like the Swarm Optimization algorithm [18], the Whale Optimization algorithm [19], and Bayesian optimization [20] are frequently used. However, while these conventional methods have proven to be widely adopted and effective, they focus on static feature extraction from individual cycles, where the predictions are easily contaminated by noise and incomplete degradation information.

Moving beyond single cycles, several studies have attempted to leverage multi-cycle information for SOH estimation. Using a dual-sliding-window strategy, Zhao *et al* [21] averaged cumulative capacity across adjacent cycles and voltage intervals within each cycle to reconstruct input features for low-sampling-rate SOH estimation. Zhang *et al* [22] developed a multi-cycle net, which first extracts intra-cycle features from consecutive cycles (k-n to k) using a GRU-transformer, and then aggregates them via a GRU to obtain inter-cycle features for predicting the SOH of the kth cycle. Huang *et al* [23] simultaneously used both intra-cycle and inter-cycle features. Intra cycle features were extracted from 1D embedding voltage sequences for SOH estimation, while inter-cycle features were obtained by applying Inception convolution and self-attention across cycles for degradation trajectory prediction. The two were then fused by cross-attention to predict RUL. Building upon the multicycle concept, Ardakani *et al* [24] further introduced a feedback mechanism that incorporates previous SOH predictions into the input, enabling nonlinear auto-regressive modeling of battery degradation. The employment of multi-cycle features enables the models to utilize richer information from adjacent cycles than single-cycle features. However, the dynamic evolution of signal similarity across different cycles remains largely unexplored.

The concept of recurrence plots, originally proposed by Eckmann *et al* [25], visually illustrates the recurring patterns in time series data. To quantitatively characterize the recurring patterns, Zbilut and Webber introduced recurrence quantification analysis (RQA), where metrics reveal the regularity, predictability, and stability of the system's dynamics. The recurrence rate (RR), for example, is defined as the density of recurrence points in the plots, measuring how often the system returns to a previously visited state and reflecting the degree of repetitiveness in system behavior. Furthermore, Marwan and Kurths extended RQA to Cross-RQA (CRQA) [26], which compares the similarity between two time sequences using cross-recurrence plots (CRPs) [27] and associated metrics. As CRQA enables the comparison between two systems, it has been applied to biomedical signal analysis [28, 29], seismic ground motion characterization [30], and ultrasonic nondestructive testing [31]. However, CRQA's application to battery degradation analysis remains largely unexplored. Xie *et al* [32] convert voltage signals into recurrence plots to extract spatiotemporal features for RUL prediction, while still relying on single-cycle features without considering cross-cycle evolution. The charge-discharge process involves inherent repeated visits to similar operating states across degradation cycles, and CRQA is designed to quantify the evolution of such recurrence structures. Therefore, CRQA is well-suited for detecting the similarity and differences of degradation trends in battery signals.

In summary, existing methods for battery SOH prediction rely on features from individual or adjacent cycles, overlooking the dynamic evolution of measurements across

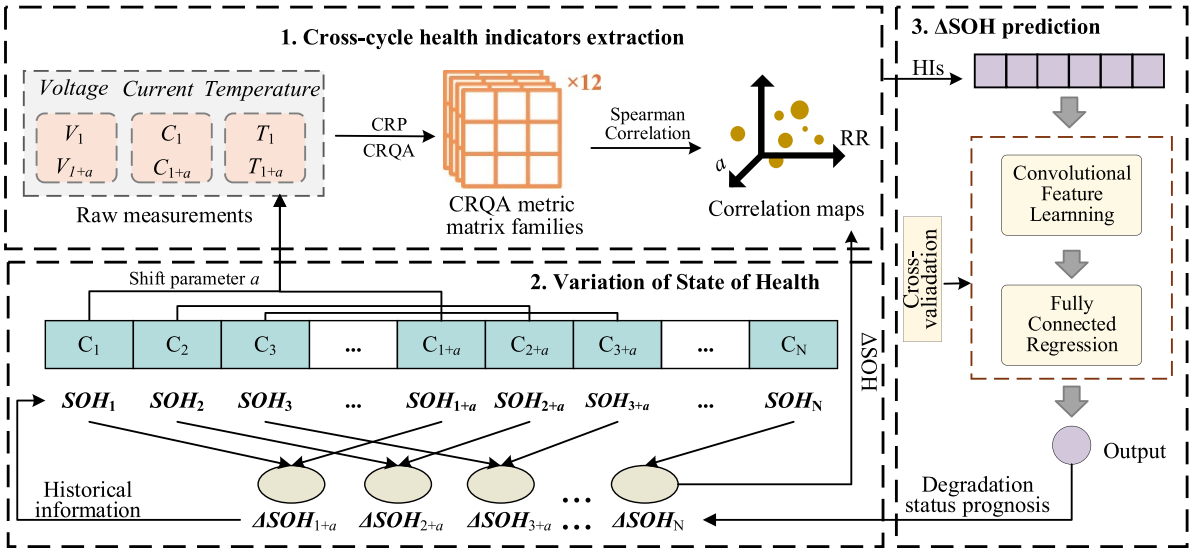


Figure 1. The framework for SOH prognosis of lithium-ion batteries based on cross-cycle HIs and CNN.

different degradation stages. Therefore, this article proposes a novel framework that estimates SOH using cross-cycle HIs extracted by CRQA, as shown in figure 1. Firstly, cross-cycle features are proposed from battery degradation signals between cycles. For discharge signals: voltage, current, and temperature, CRQA is applied to compare raw data between cycle i and cycle $i + a$, where i is the cycle index and a is the shift parameter. This yields the CRQA metric matrix families parameterized by a and recurrence rate RR. Then, the variation of SOH (ΔSOH) is introduced, and correlation maps between CRQA metrics and ΔSOH are constructed to select highly correlated metrics as HIs and identify optimal parameters. Finally, a CNN with time series cross-validation is developed to predict ΔSOH between cycles i and $i + a$. The SOH of cycle $i + a$ is then obtained by adding the predicted ΔSOH to the known SOH of cycle i.

The main contributions of this paper are summarized as follows:

(1) A CRQA based framework is proposed to quantify the evolution of raw voltage, current, and temperature signals across different cycles in battery degradation.
(2) Cross-cycle features are proposed as HIs for battery SOH estimation, instead of focusing on static features within a single charge-discharge cycle.
(3) An indirect method for SOH estimation is introduced based on the cross-cycle HIs. The SOH in a future cycle is estimated from the predicted ΔSOH, which is generated by a CNN with time series cross-validation.

This paper is organized as follows. Section 2 describes how CRQA metric matrix families are constructed from battery signals using cross-recurrence quantification and how correlation maps are built to illustrate the relationship between features and battery degradation. Section 3 presents the proposed CNN model with time series cross-validation for ΔSOH estimation. Section 4 presents the experimental results based on a NASA dataset, including implementation details of the framework and its performance evaluation. Section 5 concludes the paper with a summary of key findings.

2. Cross-cycle variability modeling for HIs extraction of lithium-ion battery degradation by CRQA

2.1. Cross-cycle variability modeling of battery operational signals by CRQA

Voltage, current, and temperature are three commonly used measurable parameters in the study of battery aging. Across battery charge-discharge cycles, each signal follows a specific trajectory under identical operating conditions. To quantify each parameter's regular time-varying pattern, vectors V, C, and T are defined by equations (1)–(3), each signal vector comprises a time-series of sampled measurements:

$$\boldsymbol{V}^i = \left[v^i(t_1)\cdots v^i(t_x)\cdots v^i(t_N)\right] \tag{1}$$

$$\boldsymbol{C}^i = \left[c^i(t_1)\cdots c^i(t_x)\cdots c^i(t_N)\right] \tag{2}$$

$$\boldsymbol{T}^i = \left[\tau^i(t_1)\cdots \tau^i(t_x)\cdots \tau^i(t_N)\right] \tag{3}$$

where $\boldsymbol{V^i}$, $\boldsymbol{C^i}$ and $\boldsymbol{T^i}$ are voltage, current and temperature vectors for the ith cycle, respectively. The elements $v^i(t_x)$, $c^i(t_x)$, and $\tau^i(t_x)$ represent the instantaneous measurements of voltage, current, and temperature at time t_x during the ith charge-discharge cycle, and N is the number of sampling points in the ith cycle.

With the increasing number of cycles, battery performance degrades continuously. This phenomenon is manifested as an earlier occurrence of specific events on each parameter's trajectory, such as the voltage reaching a fixed threshold and the temperature attaining its peak. Therefore, to quantitatively analyze the observed cross-cycle temporal shifts, this study

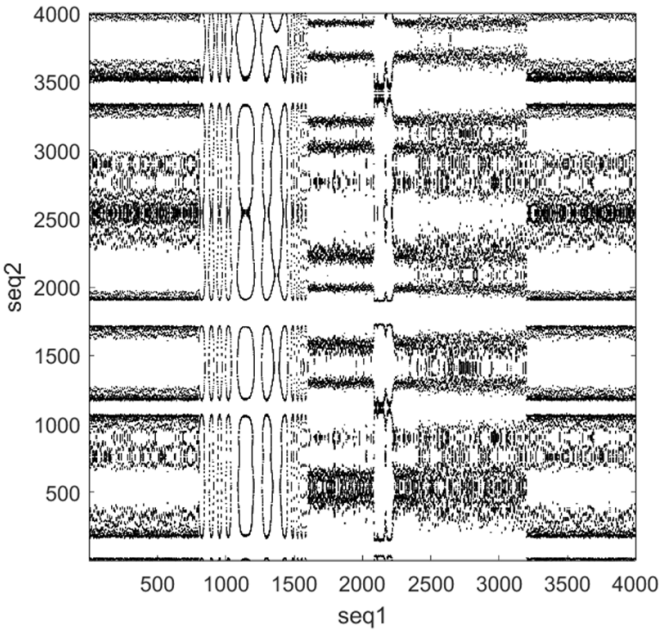


Figure 2. Cross-recurrence plot.

introduces a shift parameter, a, characterizing the variation in the trajectory of each signal across cycles. Vectors V^{i+a}, C^{i+a}, and T^{i+a} are shown in equations (4)–(6).

$$\boldsymbol{V}^{i+a} = \left[v^{i+a}(t_1)\cdots v^{i+a}(t_y)\cdots v^{i+a}(t_M)\right] \tag{4}$$

$$\boldsymbol{C}^{i+a} = \left[c^{i+a}(t_1)\cdots c^{i+a}(t_y)\cdots c^{i+a}(t_M)\right] \tag{5}$$

$$\boldsymbol{T}^{i+a} = \left[\tau^{i+a}(t_1)\cdots \tau^{i+a}(t_y)\cdots \tau^{i+a}(t_M)\right]. \tag{6}$$

As an external representation of battery degradation, the variations between signal trajectories of cycles i and $i+a$ require precise delineation and measurement. Based on the statistical analysis of diagonal, vertical, and isolated point structures in CRP, CRQA enables the comparison of two trajectories.

For any two signal vectors $(\mathbf{V}_1^i, \mathbf{V}_1^{i+a})$ defined, an $N \times M$ cross-recurrence matrix $(CR^{i,i+a})$ is constructed by computing pairwise distances between the two trajectories. For example, for voltage data, when denoting the xth observation $v^i(t_x)$ in cycle i and the yth observation $v^{i+a}(t_y)$ in cycle $i+a$, the cross-recurrence matrix assigns 1 to position (x, y) if the Euclidean distance $\left\|v^i(t_x) - v^{i+a}(t_y)\right\|$ is smaller than a predefined threshold ε, and 0 otherwise, as shown in equation (7):

$$CR_{x,y}^{i,i+a}(\varepsilon) = \Theta\left(\varepsilon - \left\|v^i(t_x) - v^{i+a}(t_y)\right\|\right), \quad x = 1,\ldots,N, y = 1,\ldots,M \tag{7}$$

where ε is a predefined threshold distance, $\left\|v^i(t_x) - v^{i+a}(t_y)\right\|$ is the Euclidean norm of vectors, and the Heaviside function Θ meets the condition: $\Theta(x<0)=0, \Theta(x>0)=1$.

The recurrence rate (*RR*), a fundamental metric in CRQA, is calculated as the density of recurrence points in the matrix, as shown in equation (8):

$$RR = \frac{1}{N \times M}\sum_{x=1}^{N}\sum_{y=1}^{M} CR^{i,i+a}. \tag{8}$$

This scalar quantifies probability that the states in cycle i recur within the ε-neighborhood of states in cycle $i+a$. To practically ensure comparability across different cycle pairs, a recurrence rate-fixed approach is adopted in this study. By specifying a target RR value first and then inversely determining the corresponding threshold ε, this approach yields the desired point density in the matrix. Therefore, by varying RR, we can modulate ε to produce a spectrum of recurrence matrices with point densities ranging from sparse to dense. The structure of the recurrence matrix, in turn, affects the value of cross-recurrence metrics calculated from it.

Then, the CRP could be obtained from the cross-recurrence matrix $CR^{i,i+a}$, where black/white points correspond to $CR_{x,y}^{i,i+a} = 1/0$, respectively. A CRP is illustrated in figure 2.

The CRP visually represents signal variations between cycles i and $i+a$. To further quantify variations across cycles, this study leverages cross-recurrence quantification metrics. These metrics are usually grouped into diagonal, vertical, horizontal, and trend types. Diagonal metrics quantify the similarity and regularity between two trajectories, including determinism (*DET*), maximum diagonal line length ($L_{\max}$), average diagonal line length (L), and entropy (*ENTR*). *DET* refers to the proportion of diagonal lines to total recurrence points, revealing the regularity of trajectory preservation between cycles i and $i+a$. A high *DET* indicates that the signal evolves in a predictable and consistent pattern as the battery ages. $L_{\max}$ and L represents the maximal and average duration during which the two trajectories

evolve similarly, respectively. *ENTR* measures the complexity of the diagonal length distribution, revealing the diversity of recurrent patterns. Their calculation formulas are shown in equations (9)–(12).

(1) Determinism

$$DET = \frac{\sum_{l_{\min}}^{N} l \cdot P(l)}{\sum_{x=1}^{N} \sum_{y=1}^{M} CR^{i,j}} \tag{9}$$

where l is the diagonal line length, $l_{\min} = 2$ is the minimum diagonal threshold (excluding isolated points), and $P(l)$ is the distribution of diagonal lines with length l.

(2) Maximum diagonal line length

$$L_{\max} = \max\left(\{ l | l \geqslant l_{\min} \}\right) \tag{10}$$

(3) Average diagonal line length

$$L = \frac{\sum_{l=l_{\min}}^{l_{\max}} l \cdot p(l)}{\sum_{l=l_{\min}}^{l_{\max}} p(l)} \tag{11}$$

where $p(l)$ is the probability distribution of diagonal lines with length l.

(4) Entropy

$$ENTR = -\sum_{l=l_{\min}}^{l_{\max}} p(l) \cdot \log_2 p(l). \tag{12}$$

Laminar related metrics describe vertical and horizontal line structures in the cross- recurrence plot, reflecting laminar states, which are periods where the signal remains relatively stable or changes slowly across the two cycles. For vertical structures, three metrics are defined: vertical laminarity (LAM_{V}), maximum vertical line length ($V_{\max}$), and vertical trapping time (TT_{V}). LAM_{V} refers to the proportion of vertical lines to total recurrence points, reflecting how frequently the signal remains stable across the two cycles. $V_{\max}$ and TT_{V} denote the maximal and average duration of such states, respectively. They are computed by equations (13)–(15).

(5) Laminarity

$$LAM_V = \frac{\sum_{v=v_{\min}}^{N} v \cdot p(v)}{\sum_{v=1}^{N} v \cdot p(v)} \tag{13}$$

where v is the vertical line length, $v_{\min} = 2$ is the minimum diagonal threshold (excluding isolated points), and $P(v)$ is the distribution of diagonal lines with length v.

(6) Maximum Vertical Line Length

$$V_{\max} = \max\left(\{ v | v > v_{\min} \}\right) \tag{14}$$

(7) Trapping Time

$$TT_V = \frac{\sum_{v=v_{\min}}^{N} v \cdot p(v)}{\sum_{v}^{N} p(v)} \tag{15}$$

where $p(v)$ is the probability distribution of diagonal lines with length v.

The horizontal counterparts, LAM_{H}, $H_{\max}$, and TT_{H}, are defined analogously and share the same physical interpretations.

$TREND_+$ and $TREND_-$ are the linear slopes of recurrence rates in the positive and negative delay regions of the recurrence plot. $TREND_+$ represents how the recurrence rate changes as the positive delay increases, while $TREND_-$ represents how the recurrence rate changes as the negative delay decreases.

(8) TREND

$$TREND = \frac{\sum_{k=1}^{N} \left(k - \bar{k}\right)\left(RR_k - \overline{RR}\right)}{\sum_{k=1}^{N} \left(k - \bar{k}\right)^2} \tag{16}$$

where RR_k is the recurrence rate of the kth diagonal (with an offset of k from the main diagonal), $\overline{RR}$ is the average value of all RR_k, and $\bar{k}$ denotes the average value of the diagonal offset quantity k.

According to the abovementioned twelve CRQA metrics, features of battery status variations could be quantified by twelve metrics $\{Q_1, Q_2, \ldots, Q_{12}\}$, each metric Q_n (n = 1, 2, 3, …,12) corresponds to: *DET,* $L_{\max}$, *L, ENTR,* LAM_{V}, TT_{V}, $V_{\max}$, LAM_{H}, TT_{H}, $H_{\max}$, $TREND_+$, $TREND_$.

2.2. Cross-cycle HIs of batteries based on cross-cycle variability modeling

In section 2.1, twelve CRQA metrics are defined by line structures in the recurrence plot. Also, shift parameter 'a' determines which two signal vectors are used for HIs by cross-recurrence quantification and recurrence rate (*RR*) serves as a threshold that directly controls the density of recurrence points in the recurrence plot. Therefore, both 'a' and 'RR' influence the values of computed CRQA metrics.

For battery degradation with a total of C complete charge-discharge cycles, signals of discharging cycles i and $i + a$ are analyzed by cross-recurrence quantification, where 'a' is an integer lag. The starting cycle index i runs from 1 to K, where $K = C - a$ ensures the paired cycle $i + a$ remains within the available cycles.

Let $Q_n(i, i + a; RR)$ denote the value of the CRQA metric Q_n between cycles i and $i + a$ at recurrence rate RR. Therefore, for a fixed a, the matrix of one specific metric $Q_n \in \{Q_1, Q_2, \ldots, Q_{12}\}$ for the voltage in battery degradation across a range of recurrence rate $\{RR_1, RR_2, \ldots, RR_k, \ldots, RR_{95}\}$ is defined as follows:

$$\mathbf{M}_n^V(a) = Q_n^V(i, i+a; RR_k), \quad i = 1, \ldots, K, \; k = 1, \ldots 95$$
$$= \begin{bmatrix} Q_n^V(1,1+a;RR_1) & Q_n^V(1,1+a;RR_2) & \cdots & Q_n^V(1,1+a;RR_{95}) \\ Q_n^V(2,2+a;RR_1) & Q_n^V(2,2+a;RR_2) & \cdots & Q_n^V(2,2+a;RR_{95}) \\ \vdots & \vdots & \ddots & \vdots \\ Q_n^V(K,K+a;RR_1) & Q_n^V(K,K+a;RR_2) & \cdots & Q_n^V(K,K+a;RR_{95}) \end{bmatrix}. \tag{17}$$

In this matrix, each row corresponds to a fixed cycle pair $(i, i+a)$ for the discharge voltage signal, which contains the value of the CRQA metric Q_n computed across all recurrence-rate thresholds from RR_1 to RR_{95}. Conversely, each column represents the value of the same metric Q_n for the same voltage signal at a fixed recurrence rate RR_k, computed across all cycle pairs $(i, i+a)$ where $i = 1, \ldots, K$.

Then, when a values from $a \in \{a_1, a_2, \ldots, a_L\}$, cross-cycle battery HIs based on varying a and RR form a family of metric matrices $\left\{M_n^V(a_l) \,|\, l = 1, 2, \ldots, L\right\}$. Similarly, metric matrices for current and temperature are obtained: $\left\{M_n^C(a_l) \,|\, l = 1, 2, \ldots, L\right\}$ and $\left\{M_n^T(a_l) \,|\, l = 1, 2, \ldots, L\right\}$. Thus, 12 CRQA matrix families are obtained for each signal, one corresponding to each CRQA metric Q_n (n = 1, 2, …, 12).

2.3. Correlation map analysis of cross-cycle HIs of batteries

The SOH is defined as the ratio of current capacity to nominal capacity, as shown in equation (18), which is a key indicator of battery performance and operational states

$$\mathrm{SOH} = \frac{C_{\mathrm{cur}}}{C_0} \tag{18}$$

where C_{cur} denotes the measured capacity at the current cycle, and C_0 represents the rated capacity at the defined initial cycle.

Most existing SOH prediction models rely on current cycle signals. However, the degradation of battery capacities has great uncertainties, and this method is unable to grasp the uncertainty hidden in historical status information. Therefore, the variation of SOH (ΔSOH) between any two cycles i and $i+a$ is introduced in this section. The vector of ΔSOH for K cycles is defined as:

$$\boldsymbol{\Delta SOH}^{(a)} = \begin{bmatrix} \Delta\mathrm{SOH}_{1+a}^{(a)} \\ \Delta\mathrm{SOH}_{2+a}^{(a)} \\ \vdots \\ \Delta\mathrm{SOH}_{K+a}^{(a)} \end{bmatrix} = \begin{bmatrix} \mathrm{SOH}_{1+a} - \mathrm{SOH}_1 \\ \mathrm{SOH}_{2+a} - \mathrm{SOH}_2 \\ \vdots \\ \mathrm{SOH}_{K+a} - \mathrm{SOH}_K \end{bmatrix} \tag{19}$$

where each element $\Delta\mathrm{SOH}_{i+a}^{(a)}$ denotes the variation of SOH between cycle i and $i+a$.

As shown in section 2.2, the value of each CRQA metric depends on both the shift parameter a and the recurrence rate RR. Furthermore, different CRQA metrics potentially exhibit varying levels of correlation with ΔSOH. Therefore, a preliminary screening of both the metrics and the a-RR candidates is necessary.

Firstly, for a specific CRQA metric matrix M_n^V, where recurrence rate (RR) is an independent variable and a fixed shift parameter a, a correlation vector is constructed:

$$\boldsymbol{\rho}_n^V(a) = \begin{bmatrix} \rho_n^V(a;RR_1) & \rho_n^V(a;RR_2) & \cdots & \rho_n^V(a;RR_{95}) \end{bmatrix} \tag{20}$$

where $\rho_n^V(a;RR_k) = Spearman\left(M_n^V(a)[:,k], \boldsymbol{\Delta SOH}^{(a)}\right)$, and $M_n^V(a)[:,k]$ denotes the kth column of the matrix (k = 1, 2, …, 95).

Then, by varying the shift parameter a over the set of $\{a_1, a_2, \ldots, a_L\}$, above procedure is repeated for each value. Stacking the resulting row vectors forms a correlation map:

$$\rho_n^V = \begin{bmatrix} \rho_n^V(a_1) \\ \rho_n^V(a_2) \\ \vdots \\ \rho_n^V(a_L) \end{bmatrix}$$
$$= \begin{bmatrix} \rho_n^V(a_1;RR_1) & \rho_n^V(a_1;RR_2) & \cdots & \rho_n^V(a_1;RR_{95}) \\ \rho_n^V(a_2;RR_1) & \rho_n^V(a_2;RR_2) & \cdots & \rho_n^V(a_2;RR_{95}) \\ \vdots & \vdots & \ddots & \vdots \\ \rho_n^V(a_L;RR_1) & \rho_n^V(a_L;RR_2) & \cdots & \rho_n^V(a_L;RR_{95}) \end{bmatrix}. \tag{21}$$

This matrix ρ_n^V comprehensively displays the correlation between the voltage signal metric Q_n and the variation of SOH, together with two parameters, a and RR.

Finally, based on the analysis of correlation maps, signal-metric pairs with low ρ will not be adopted. Also, the impact of both the shift parameter, a, and the recurrence rate, RR, on the correlation matrix could be examined to identify the optimal parameter settings.

3. CNN prediction model with time series cross-validation

This section describes the CNN employed for battery SOH estimation. Additionally, the time series cross-validation strategy is adopted for hyperparameter tuning, and the architecture of the model is illustrated in figure 3.

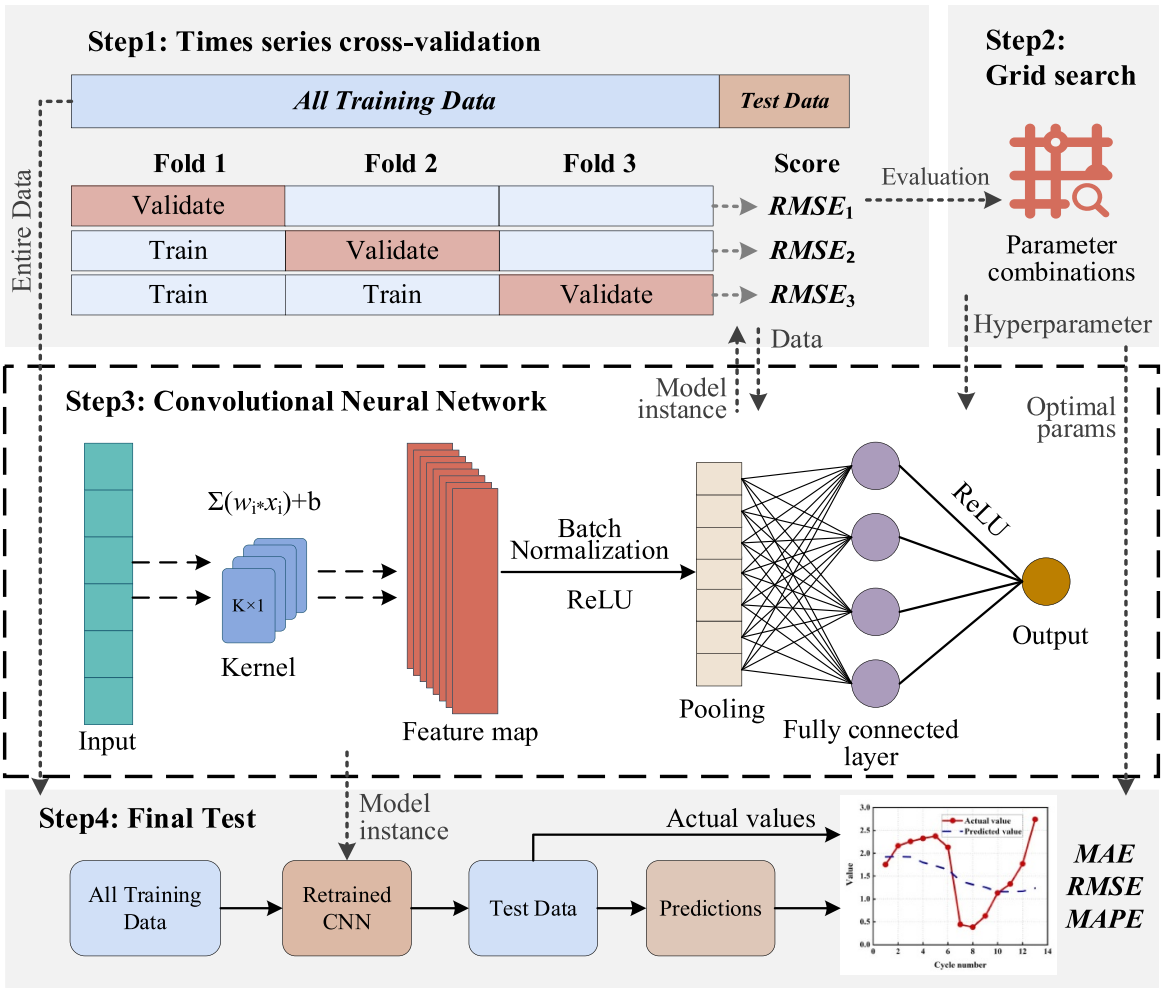


Figure 3. CNN architecture under time-series cross-validation.

According to section 2.3, CRQA metrics with high correlation are retained for prediction. These retained features, derived from CRPs, contain rich information that reflects battery degradation. By leveraging convolutional kernels, CNNs [33, 34] operate on local regions of the feature vector, allowing it to capture local dependencies among neighboring features. This makes it suitable for learning CRP-based metrics and contributes to the reliability of data-driven prognostic predictions [35]. Additionally, time series cross-validation, serving as the evaluation engine within a grid search framework, is employed to systematically optimize the hyperparameters with chronological splits to avoid data leakage from future cycles.

Let $\{(x_t, y_t)\}_{t=1}^{N}$ be a time ordered sequence, where $x_t \in \mathbb{R}^d$ is the input feature vector at time t, $y^t \in \mathbb{R}$ is the corresponding target value. Standard K-fold cross-validation assumes exchangeable samples and is therefore inappropriate for time series data. To respect the temporal order in battery degradation, a time series cross-validation scheme is employed in this study. Let the training set size be M. Define K validation splits such that for each $k = 1, \ldots, K$:

$$\mathcal{T}_k = \{(x_t, y_t)\}_{t=1}^{T_k}, \quad \mathcal{V}_k = \{(x_t, y_t)\}_{t=T_k+1}^{T_{k+1}} \tag{22}$$

where T_k denotes the last index of the training set of fold k, $T_1 < T_2 < \cdots < T_{K+1} = M$. The validation set $\mathcal{V}_k$ always follows the training set $\mathcal{T}_k$ in time, preventing future information leakage.

The root mean error for split k is

$$e_k = \sqrt{\frac{1}{|\mathcal{V}_k|} \sum_{(x_t, y_t) \in \mathcal{V}_k} (\hat{y}_t - y_t)^2}. \tag{23}$$

The overall cross-validation objective is

$$\mathcal{L}_{\mathrm{CV}} = \frac{1}{K} \sum_{k=1}^{K} e_k. \tag{24}$$

Grid search is performed over hyperparameters including kernel size, number of filters, and dropoutRate. Then, for each hyperparameter combination, a CNN with that configuration is trained on $\mathcal{T}_k$ and validated on $\mathcal{V}_k$ for each fold of $k = 1, \ldots, K$. Then per-fold e_k and the average cross-validation loss $\mathcal{L}_{\mathrm{CV}}$ is computed. The combination achieving the smallest $\mathcal{L}_{\mathrm{CV}}$ is selected as the optimal configuration.

Each input $x_t \in \mathbb{R}^d$ for the CNN is reshaped into a tensor of size $d \times 1 \times 1$ to match the expected input format of the

convolutional layer. The first convolutional operation is then applied as follows:

$$Z^{(1)} = W^{(1)} * X + b^{(1)} \tag{25}$$

where $W^{(1)}$ is the filter bank, $b^{(1)}$ is the bias term, and $*$ represents the convolution operation. This transformation yields a feature map:

$$Z^{(1)} \in \mathbb{R}^{d\times 1\times D} \tag{26}$$

with D filters.

To stabilize and accelerate training, a batch normalization layer is introduced:

$$\hat{Z}^{(1)} = \gamma \frac{Z^{(1)} - \mu}{\sqrt{\sigma^2 + \in}} + \beta \tag{27}$$

where μ and σ^2 are the batch mean and variance, and γ, and β are learnable affine parameters.

Subsequently, the ReLU activation introduces the nonlinearity.

$$A^{(1)} = \mathrm{Re}LU\left(\hat{Z}^{(1)}\right) = \max\left(0, \hat{Z}^{(1)}\right). \tag{28}$$

A pooling layer is applied to down-sample the feature maps:

$$P^{(1)} = \mathrm{avgpool}\left(A^{(1)}\right). \tag{29}$$

The extracted features are then integrated through a fully connected layer

$$Z^{(2)} = W^{(2)}A^{(1)} + b^{(2)} \tag{30}$$

$$A^{(2)} = \mathrm{Re}LU\left(Z^{(2)}\right). \tag{31}$$

Finally, the model produces the prediction through an output layer:

$$\hat{y}_t = W^{(3)}A^{(2)} + b^{(3)}. \tag{32}$$

With the predicted $\Delta\mathrm{SOH}_{i+a}$ obtained by CNN, the final SOH at cycle $i + a$ is obtained by adding this predicted value to the SOH at cycle i, as formulated below:

$$\mathrm{SOH}_{i+a} = \mathrm{SOH}_i + \Delta\mathrm{SOH}_{i+a}. \tag{33}$$

To assess the proposed CNN model, the errors between the estimated SOH values and the actual SOH values are evaluated using mean absolute error (MAE) and root mean square error (RMSE) [36], which are computed according to equations (34) and (35).

$$\mathrm{MAE} = \frac{1}{n}\sum_{i=1}^{n}|y_i - \hat{y}| \tag{34}$$

$$\mathrm{RMSE} = \sqrt{\frac{1}{n}\sum_{i=1}^{n}(y_i - \hat{y}_i)^2}. \tag{35}$$

4. Experimental analysis

4.1. Cross-cycle HIs extraction under varying a and RR

In this study, the lithium-ion battery dataset (B0005) from the NASA Ames Prognostics Data Repository is leveraged. The battery is an 18 650-type lithium-ion cell with a rated capacity of 2 Ah. The charging protocol consists of a constant current phase at 1.5 A until the voltage reaches 4.2 V, followed by a constant voltage phase until the current drops to 20 mA. The discharging protocol applies a constant current until the voltage falls to 2.7 V. The dataset provides measurements of voltage, current, temperature and capacity after every charge-discharge cycle.

According to equation (19), the ΔSOH curve is governed by the shift parameter a. To ensure an adequate sample size and CRQA HIs achieve the highest correlation with ΔSOH, the shift parameter a is set from 28 to 31 in this study. Within this range, the extracted HIs achieve correlations up to 91%.

The ΔSOH curves for $a = 28$, 29, 30, and 31 are shown in figure 4. Notably, the four curves exhibit a pronounced pattern: first decreases to a minimum and then slowly recovers. This phenomenon reflects that the B0005 battery degradation rate first increases rapidly and then decreases gradually. Furthermore, as a varies from 28 to 31, the slope of the ΔSOH curve becomes progressively steeper.

For HI derivation related to battery degradation, CRQA metric matrix families for current, voltage, and temperature are constructed based on the methodology in sections 2.1 and 2.2. Unlike ΔSOH's dependency on shift parameter a, the derivation of HIs is determined by both the shift parameter a and the recurrence rate, RR. For a recurrence rate of 5%, figure 5 shows how the CRQA metrics *ENTR* and TT_{H} of voltage vary across all cycles as a increases from 28 to 31.

A clear divergence is observed between the shapes of *ENTR* and $TT_{\mathrm{H,}}$ indicating the distinct response patterns for battery degradation in each CRQA metric. Then, as a increases from 28 to 31, each curve retains its overall trend but drifts rightward along the cycle axis.

For shift parameter $a = 30$, figure 6 shows the *ENTR* and TT_{H} curves of signal voltage, with recurrence rate values of $\{5\%, 10\%, 15\%, \ldots, 95\%\}$. In figure 6, as RR ranges from 5% to 95% in steps of 5%, the *ENTR* curve first shifts upward, then downward along the vertical axis, whereas the TT_{H} curve exhibits a consistent upward shift across the same RR range.

Given that the behavior of CRQA metrics is highly sensitive to the choice of a and RR, selecting the optimal values for these two parameters is crucial for constructing effective prognostic features.

4.2. Parameter selection based on correlation maps

In section 4.1, we construct CRQA metric matrices. These matrices reveal the distinct response patterns of CRQA metrics to variations in the shift parameter, a, and the recurrence rate, RR. To select optimal parameters and correlated metrics, correlation matrices for three signals and 12 metrics

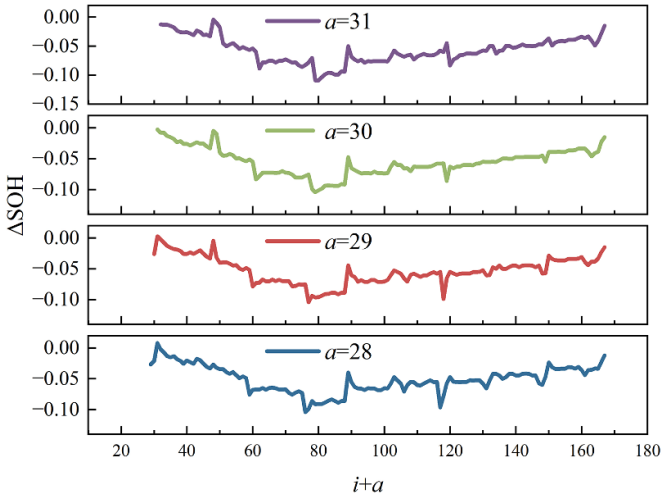


Figure 4. ΔSOH curves for different a values.

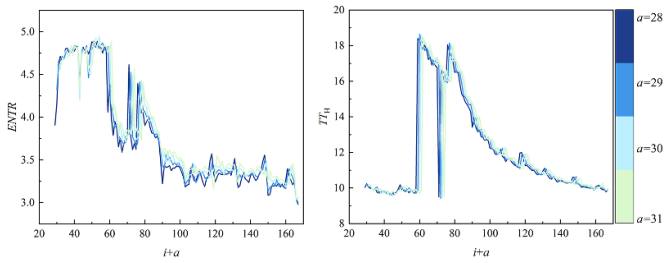


Figure 5. *ENTR* and TT_{H} curves for different a values.

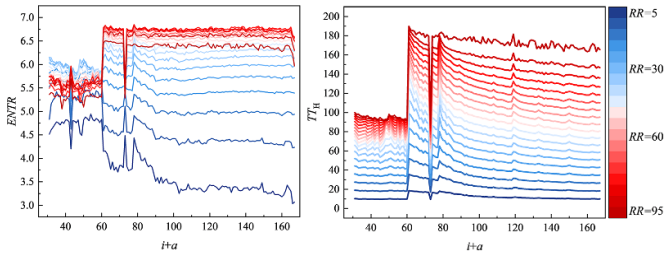


Figure 6. *ENTR* and TT_{H} curves for different RR values.

are constructed according to equation (21). Only the values of a that achieve correlation coefficients of up to 91% are retained for subsequent parameter and metric selection. Then 3D correlation maps are generated by first unfolding the two-dimensional correlation matrix into three column vectors, representing the shift parameter, a, the recurrence rate, *RR*, and the corresponding Spearman correlation coefficient ρ, respectively. Each point in the plot thus corresponds to a unique parameter pair (a, *RR*). Twelve correlation maps of voltage are shown in figure 7.

For each a value in the range of 28–31, we further examine RR from 1% to 95%. Metric-RR combinations with correlation coefficients exceeding 0.85, 0.86, 0.87, 0.88, 0.89, 0.90, and 0.91 are selected as inputs for subsequent prediction. Tables 1–4 present the set of selected parameters and metrics for $a = 28, 29, 30, 31$.

To further validate the generalization of the proposed cross-cycle method across different battery datasets, we additionally applied the feature extraction procedure to multiple cells from the Oxford battery dataset. The correlated features and their corresponding parameters are partially presented in table 5.

Specifically, the extracted CRQA features exhibit a strong correlation with ΔSOH, with the highest correlation reaching 95%. Due to the limited number of cycles in the Oxford dataset, this analysis focuses on feature-level validation.

4.3. Prediction results and model comparison

Based on section 3, the very end of the battery dataset is used as the test set. We also employ LSTM, SVR, LSTM-Attention, and CNN-LSTM-Attention as comparison models. The prediction curves of the optimal threshold ρ under each value of a are shown in figures 8–11. In each figure, subfigure (a) shows the model's direct prediction results for ΔSOH from cycle i to $i + a$, and subfigure (b) shows the SOH results at cycle $i + a$, obtained by adding the predicted ΔSOH to the SOH of cycle i.

As illustrated in figures 8 to 11, both the SOH and ΔSOH of the battery exhibit a fluctuating trend, and the predicted values from the models are consequently subject to fluctuations. Meanwhile, the prediction curves of CNN-LSTM-Attention in figure 9, CNN in figure 10, and LSTM in figure 11, shown as brown, green, and blue lines, largely coincide with the original degradation trajectory. LSTM achieves stable performance across all values of a. SVR and LSTM-Attention show the largest deviation from the original trajectories. Notably, all the performances are sensitive to the shift parameter a.

The prediction performances are quantitatively compared in table 6, where MAE and RMSE are reported for shift parameters $a = 28, 29, 30, 31$.

Due to the linear relationship between ΔSOH and SOH, the MAE and RMSE values remain identical. The CNN achieves the lowest MAE of 0.2965% at $a = 31$, while the CNN-LSTM-Attention model achieves the lowest RMSE of 0.4156% at $a = 29$. We attribute this to the CNN's spatiotemporal feature

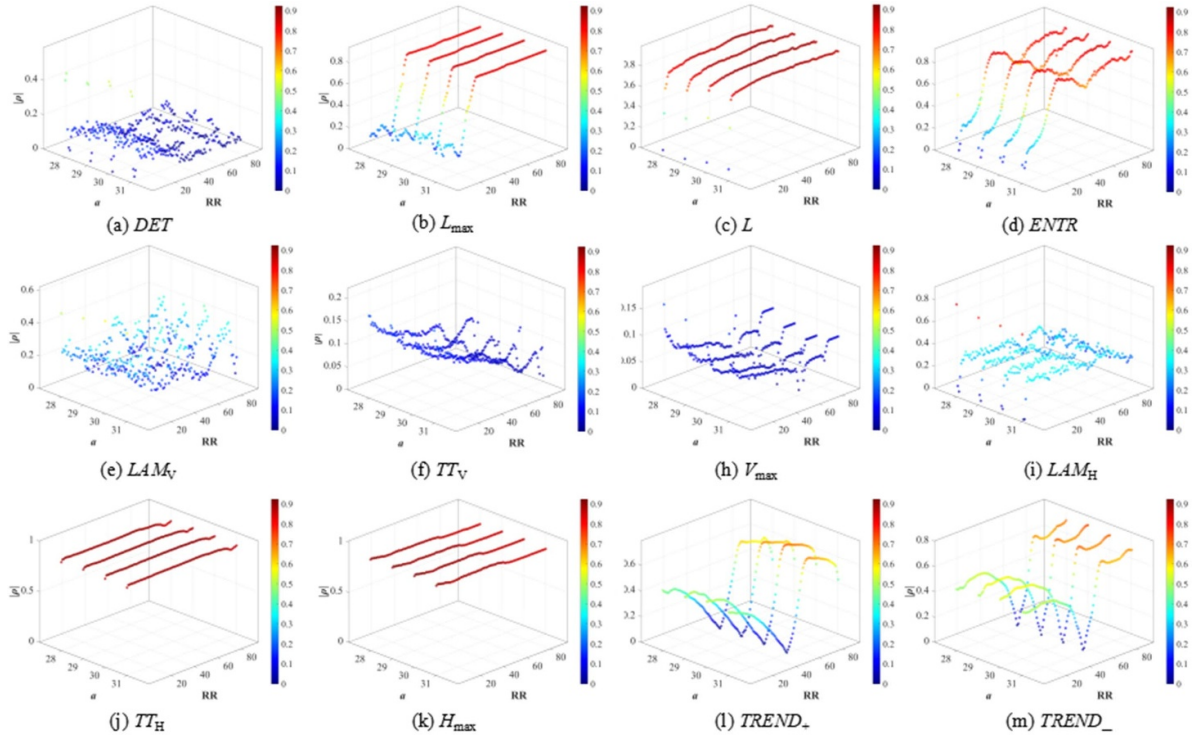


Figure 7. Twelve correlation maps of voltage.

Table 1. Feature selection results for $a = 28$.

Signal	*RR* (%)	CRQA metric (HI)	ρ (%)
Voltage	91	TREND$_-$	91.32
Temperature	2	H_{max}	91.79
	64	TT_H	90.71
	65	L	89.3

Table 2. Feature selection results for $a = 29$.

Signal	*RR* (%)	CRQA metric (HI)	ρ (%)
Current	94	H_{max}	86.23
	86	TREND$_-$	87.3
Voltage	48	TT_H	88.17
	7	H_{max}	88.36
	92	TREND$_-$	91.39
Temperature	2	H_{max}	92.19
	67	L	90.24
	68	TT_H	91.14

Table 3. Feature selection results for $a = 30$.

Signal	RR (%)	CRQA metric (HI)	ρ (%)
Current	91	H_{max}	86.57
	86	TREND$_-$	86.31
Voltage	49	TT_H	88.44
	15	H_{max}	89.18
	78	L	86.23
	42	TREND$_-$	92.36
	86	TREND$_+$	88.64
Temperature	2	H_{max}	92.38
	64	L	90.16
	56	TT_H	91.41
	63	L_{max}	85.27

Table 4. Feature selection results for $a = 31$.

Signal	*RR* (%)	CRQA metric (HI)	ρ (%)
Voltage	42	TREND$_-$	91.75
Temperature	3	H_{max}	90.70
	64	TT_H	90.55

extraction capability. In contrast, the LSTM model achieves relatively stable and competitive performance across all values of a. Collectively, the above results demonstrate that the proposed cross-cycle prediction method is feasible and effective for battery SOH prediction.

We select the optimal prediction results under each value of a for comparison with the existing non-cross-cycle prediction methods. All comparisons are conducted on the same battery dataset. The quantitative results are presented in table 7. Our method achieves a minimal MAE of 0.2965% and a minimal RMSE of 0.4156%. The MAE and RMSE values reported by Lin *et al* [7] and Zhang *et al* [37] are higher than almost all test conditions of our method, which demonstrates the feasibility of our cross-cycle method.

Table 5. Correlation results on the Oxford dataset.

Signal	*RR* (%)	CRQA metric	ρ (%)
Voltage	5	ENTR	94.8
	40	L	93.36
	15	LAM_{H}	85.49
Temperature	55	$H_{\max}$	95.12
	65	$L_{\max}$	90.11

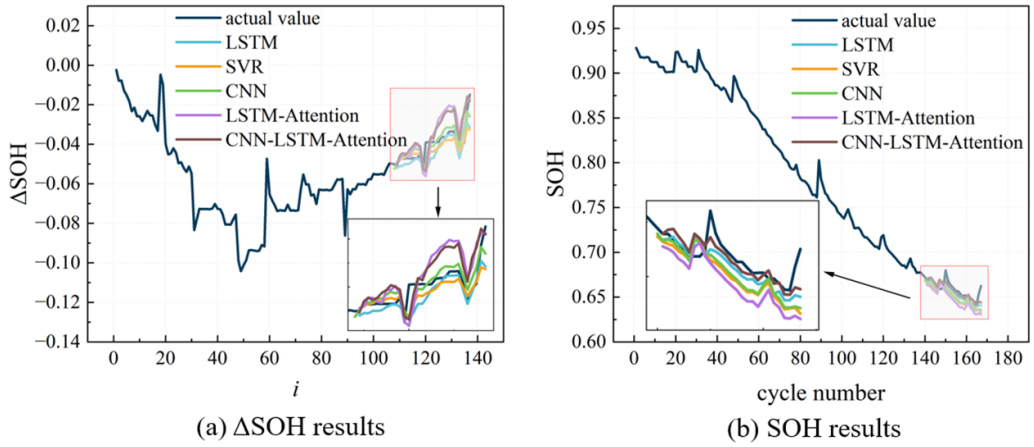


Figure 8. Prediction curves for shift parameter $a = 28$.

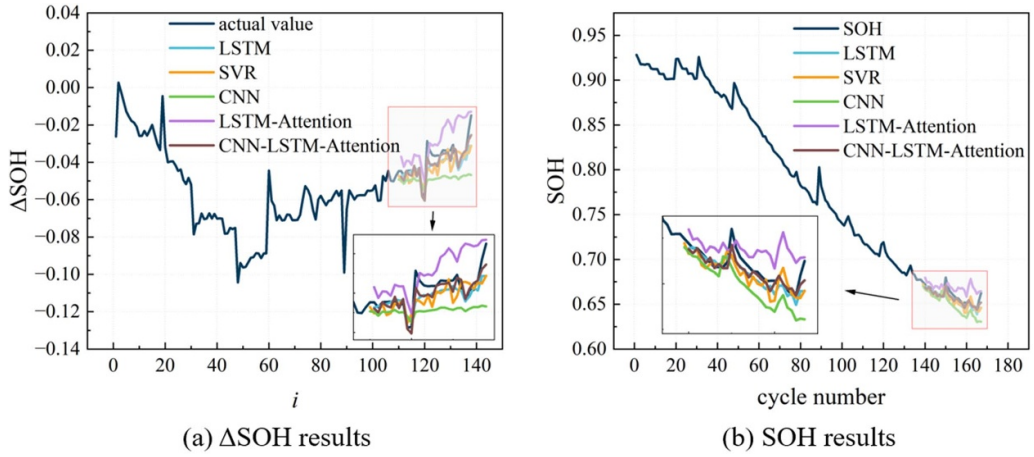


Figure 9. Prediction curves for shift parameter $a = 29$.

4.4. Sensitivity analysis of correlation threshold

Based on the three best-performing models identified in section 4.3, the impact of the correlation threshold on prediction performance is further analyzed. Table 8 summarizes the prediction results for correlation thresholds ranging from 0.85 to 0.91, with the value of a fixed at its optimal setting for each algorithm.

When the correlation threshold is set to 0.91, the performance of CNN drops abruptly. This is because the high threshold of 0.91 retains too few CRQA metrics for CNN to extract meaningful spatiotemporal patterns. Apart from this extreme threshold, CNN outperforms LSTM and CNN-LSTM-Attention and achieves the best and most stable performance. CNN-LSTM-Attention shows a gradual performance decline as the threshold increases, whereas LSTM performs poorly at the threshold of 0.88. In general, the correlation threshold significantly affects the HIs quality input to the model, yet CNN exhibits stable performance due to its inherent spatiotemporal feature extraction capability.

4.5. Ablation study

To verify the contribution of each component in the proposed framework, we conducted extensive ablation studies on our optimal CNN model. As shown in table 9, replacing the CNN with a simple MLP increases the MAE from 0.2965% to

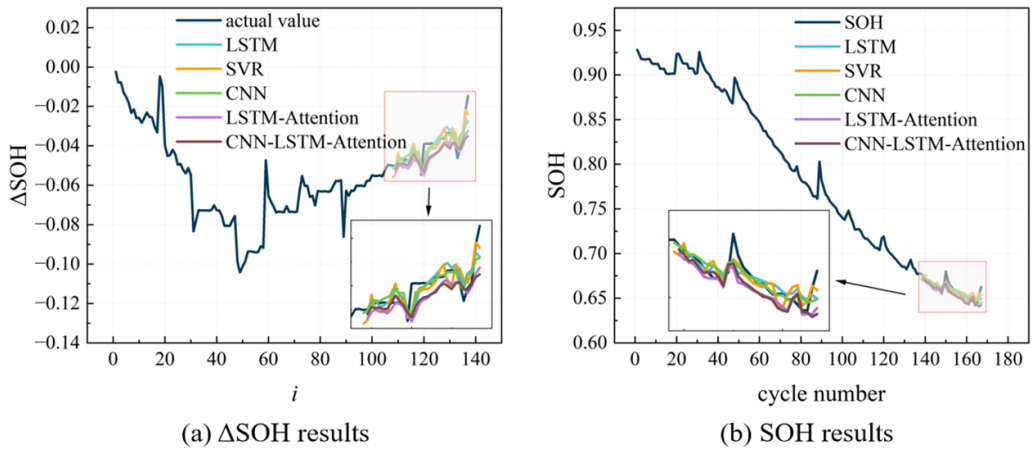


Figure 10. Prediction curves for shift parameter $a = 30$.

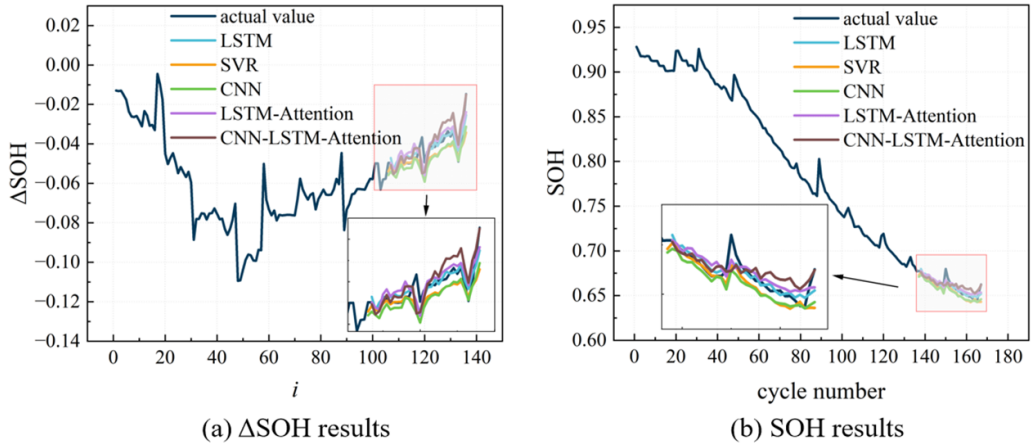


Figure 11. Prediction curves for shift parameter $a = 31$.

Table 6. Prediction performance for $a = 28$, 29, 30, and 31 (%).

a		LSTM	SVR	CNN	LSTM-Attention	CNN-LSTM-Attention
28	MAE	0.5585	0.8729	0.7674	1.1907	0.4259
	RMSE	0.7454	1.0791	0.9770	1.3618	0.5892
29	MAE	0.4298	0.5922	1.069	1.0752	0.3158
	RMSE	0.5884	0.7414	1.2672	1.2682	0.4156
30	MAE	0.359	0.4116	0.2965	0.5235	0.5004
	RMSE	0.4962	0.4895	0.4437	0.675	0.6754
31	MAE	0.3116	0.4347	0.5379	0.3994	0.4602
	RMSE	0.4415	0.6210	0.6735	0.4907	0.6121

0.643%. When the time-series cross validation is removed and a set of parameters is manually selected, the prediction accuracy decreases but remains at an acceptable level. In contrast, when the cross-cycle features are directly used to predict SOH instead of ΔSOH, the model performance deteriorates significantly, resulting in MAE of 2.5914% and RMSE of 2.9344%.

These results confirm that each component of the proposed framework contributes positively to the overall prediction performance. Among all modules, predicting ΔSOH instead of SOH yields the most significant performance gain, indicating the indispensable role of ΔSOH prediction in our cross-cycle framework.

Table 7. Performance comparison with the single-cycle prediction method (%).

		MAE	RMSE
our framework	$a = 28$	0.4259	0.5892
	$a = 29$	0.3158	0.4156
	$a = 30$	0.2965	0.4437
	$a = 31$	0.3116	0.4115
Lin *et al* [7]		0.69	0.87
Zhang *et al* [37]		0.34	0.64

Table 8. Model performance under different correlation thresholds (%).

	$a = 29$	CNN-LSTM -Attention	$a = 30$	CNN	$a = 31$	LSTM
	MAE	RMSE	MAE	RMSE	MAE	RMSE
0.85	0.3102	0.4291	0.2965	0.4437	0.3654	0.5235
0.86	0.3158	0.4156	0.4149	0.6016	0.3654	0.5235
0.87	0.4479	0.6178	0.5208	0.7374	0.4469	0.6111
0.88	0.7231	0.8911	0.5208	0.7374	0.7936	1.0176
0.89	0.9229	1.0948	0.3455	0.4637	0.3116	0.4415
0.90	0.9229	1.0948	0.3168	0.4533	0.3116	0.4415
0.91	1.1488	1.3295	0.9232	1.0591	0.3606	0.4614

Table 9. Results of ablation experiments (%).

	MAE	RMSE
Full CNN	0.2965	0.4437
MLP substitute	0.643	0.8159
without TSCV	0.3186	0.4748
direct SOH	2.5915	2.9344

5. Conclusions

This research proposes a novel cross-cycle framework that leverages HIs extracted by CRQA to estimate battery SOH degradation. Unlike conventional methods, the similarity of signals from different cycles is quantified in this method, and this approach provides a new perspective on battery degradation by explicitly modeling cross-cycle dynamic relationships. A CNN trained with time series cross-validation achieves an MAE of 0.2965% and an RMSE of 0.4156% on the NASA battery dataset, confirming the effectiveness of this cross-cycle framework. The comparison with MLP, LSTM, and CNN-LSTM-Attention shows that the proposed cross-cycle framework is capable of achieving competitive performance against these widely adopted models. Moreover, the stability of the CNN observed in the sensitivity analysis of the correlation threshold highlights its advantage in extracting informative features from CRQA metrics.

In summary, this research proposes a feasible indirect framework that explores the evolution of raw measurements in battery degradation, realizing the accurate estimation of SOH through cross-cycle features and the prediction of ΔSOH. Despite the promising results, there is still room for further improvement. In future work, more cross-cycle features could be explored to enhance the characterization of battery degradation, such as statistical features, entropy measures, and frequency features between pairs of cycles. Additionally, this research relies on correlation maps to manually select the optimal shift parameter a and recurrence rate RR. Future research could incorporate more efficient algorithms to reduce computational cost.

Acknowledgment

The work was supported by the National Natural Science Foundation of China [72571249, 72201250], the Henan Province Postdoctoral Research Project, the Key Scientific and Technological Project of Henan Province [252102221047], and the Henan Provincial Soft Science Research Program [252400411175].

References

[1] Liu Y, Chen H, Yao L, Ding J, Chen S and Wang Z 2025 A physics-guided approach for accurate battery SOH estimation using RCMHCRE and BatteryPINN *Adv. Eng. Inform.* **65** 103211

[2] Liu Y, Liu C, Liu Y, Sun F, Qiao J and Xu T 2023 Review on degradation mechanism and health state estimation methods of lithium-ion batteries *J. Traffic Transp. Eng. (Engl. Ed.)* **10** 578–610

[3] Mei W, Li H, Zhao C, Sun J and Wang Q 2020 Numerical study on thermal characteristics comparison between charge and discharge process for lithium ion battery *Int. J. Heat Mass Transfer* **162** 120319

[4] Liu Y and Wang X-L 2025 Warranties of batteries: requirements, state-of-the-art, relevant analysis methods, and research perspectives *J. Reliab. Sci. Eng.* **1** 032003

[5] Zio E 2025 Advances in reliability analysis and risk assessment for enhanced safety *J. Reliab. Sci. Eng.* **1** 013002

[6] Wang F, Zhao Z, Zhai Z, Shang Z, Yan R and Chen X 2023 Explainability-driven model improvement for SOH estimation of lithium-ion battery *Reliab. Eng. Syst. Saf.* **232** 109046

[7] Lin Y, Zhou L, Yan J and He S 2025 A hybrid data-driven model for state of health estimation of lithium-ion battery with capacity recovery *Eng. Appl. Artif. Intell.* **161** 112146

[8] Wang Y, Guo S, Cui Y, Deng L, Zhao L, Li J and Wang Z 2025 A comprehensive review of machine learning-based state of health estimation for lithium-ion batteries: data, features, algorithms, and future challenges *Renew. Sustain. Energy Rev.* **224** 116125

[9] Sun H, Sun J, Zhao K, Wang L and Wang K 2022 Data-Driven ICA-Bi-LSTM-Combined Lithium Battery SOH Estimation *Math. Probl. Eng.* **2022** 1–8

[10] Chen J, Hu Y, Zhu Q, Rashid H and Li H 2023 A novel battery health indicator and PSO-LSSVR for LiFePO4 battery SOH estimation during constant current charging *Energy* **282** 128782

[11] Nguyen C D and Bae S J 2023 Equivalent circuit simulated deep network architecture and transfer learning for remaining useful life prediction of lithium-ion batteries *J. Energy Storage* **71** 108042

[12] Wen J, Chen X, Li X and Li Y 2022 SOH prediction of lithium battery based on IC curve feature and BP neural network *Energy* **261** 125234
[13] Xia F, Dong Q, Xia L, An Z, Xia Z and Gong C 2025 Health state estimation of retired batteries based on physical constraints *Eng. Appl. Artif. Intell.* **162** 112390
[14] Chae S G and Bae S J 2025 An adaptive mixture prior in Bayesian convolutional autoencoder for early detecting anomalous degradation behaviors in lithium-ion batteries *Reliab. Eng. Syst. Saf.* **259** 110926
[15] Zhang C, Luo L, Yang Z, Zhao S, He Y, Wang X and Wang H 2023 Battery SOH estimation method based on gradual decreasing current, double correlation analysis and GRU *Green. Energy Intell. Transp.* **2** 100108
[16] Mu G, Wei Q, Xu Y, Li J, Zhang H, Yang F, Zhang J and Li Q 2025 State of health estimation of lithium-ion batteries based on feature optimization and data-driven models *Energy* **316** 134578
[17] Singh A, Singh S, Kamboj R K and Bala A 2025 Explainable OptiCNN-SLSTM hybrid model for enhanced lithium-ion battery state of health prediction *Sci. Rep.* **15** 44364
[18] Chen K, Li J, Liu K, Bai C, Zhu J, Gao G, Wu G and Laghrouche S 2024 State of health estimation for lithium-ion battery based on particle swarm optimization algorithm and extreme learning machine *Green. Energy Intell. Transp.* **3** 100151
[19] Li H, Wang S, Yang L, Zhou Z, Meng Y, Zhang W, Shuan Z, Li Y and Lv F 2025 SOH estimation method for lithium-ion battery packs under real-world operating conditions based on a new attenuated model without additional experiments *Energy* **330** 136802
[20] Ding P, Xia M, Wang X, Pan H, Gao Q, Guo W, Shi P and Min Y 2025 Advanced lithium-ion battery health state estimation using a Bayesian optimization hybrid neural network model *J. Energy Storage* **123** 116562
[21] Zhao L, Wang Z, Ma Z and Li Y 2024 An On-line SOH estimation method for power battery under low sampling rate *J. Energy Storage* **83** 110695
[22] Zhang X, He T, Zhu W, Wang S, Zeng J, Xu Q and Niu Y 2023 A SOH estimation model for energy storage batteries based on multiple cycle features *Energy Storage Sci. Technol.* **12** 3488–98
[23] Huang X, Liang C, Tao S, Che Y, Bian N, Zhang J, Wang R, Zhang Y, Xia B and Zhang X 2026 IC2ML: unified battery state-of-health, degradation trajectory and remaining useful life prediction via intra-cycle and inter-cycle enhanced machine learning *J. Power Sources* **666** 239148
[24] Ardakani A H, Abdollahian S A and Abdollahi F 2024 NARX transformer: a dynamic model for leveraging multicycle data in long-term battery state of health estimation *IEEE Trans. Instrum. Meas.* **73** 1–8
[25] Eckmann J-P, Kamphorst S O and Ruelle D 1987 Recurrence plots of dynamical systems *Europhys. Lett. EPL* **4** 973–7
[26] Marwan N and Kurths J 2002 Nonlinear analysis of bivariate data with cross recurrence plots *Phys. Lett. A* **302** 299–307
[27] Marwan N, Thiel M and Nowaczyk N R 2002 Cross recurrence plot based synchronization of time series *Nonlinear Process. Geophys.* **9** 325–31
[28] Meyers A, Buqammaz M and Yang H 2020 Cross-recurrence analysis for pattern matching of multidimensional physiological signals *Chaos Interdiscip. J. Nonlinear Sci.* **30** 123125
[29] Yang H Hui Yang 2011 Multiscale recurrence quantification analysis of spatial cardiac vectorcardiogram signals *IEEE Trans. Biomed. Eng.* **58** 339–47
[30] García S R, Romo M P and Figueroa-nazuno J 2013 Characterization of ground motions using recurrence plots *Geofísica Int.* **52** 209–27
[31] Wang Z, Yang C L, Zhou X J and Teng Y H 2019 Identification of localized void defects in composite by recurrence quantification analysis of ultrasonic backscattered signal *Russ. J. Nondestruct. Test.* **55** 192–201
[32] Xie Y, Li J, Zou W and Mao L 2024 Prediction of remaining useful life for lithium-ion battery using recurrence plot analysis *Energy Storage Sci. Technol.* **13** 3630–41
[33] Gao F, Chen Y, Lin J, Zhu Y, Miao Y and Tian J 2026 Mel spectrogram–driven deep learning framework for acoustic emission-based manufacturing monitoring in wire arc additive manufacturing *J. Reliab. Sci. Eng.* **2** 025301
[34] Lin M, Ke L, Meng J, Wu J and Stroe D-I 2025 An ensemble convolutional neural network based transfer learning framework for achievable lithium-ion battery health perception in flexible charging procedure *IEEE/ASME Trans. Mechatron.*. 30 5420–31
[35] Liu J, Zheng S, Chen Y, Xu D, Wang C, Xiang W, Xiao X and Lin J 2026 Review on reliability of intelligent autonomous systems *J. Reliab. Sci. Eng.* **2** 012002
[36] Lin M, Huang J, Meng J and Wu J 2025 Lithium-ion battery sensorless temperature estimation via integrating data enhancement and transfer learning *IEEE Trans. Ind. Electron.* **72** 11274–84
[37] Zhang C, Tu L, Yang Z, Du B, Zhou Z, Wu J and Chen L 2025 A CMMOG-based lithium-battery SOH estimation method using multi-task learning framework *J. Energy Storage* **107** 114884



Le Wang received a BS degree in industrial engineering from Zhengzhou University, Zhengzhou, China, in 2024. She is currently pursuing an MS degree in management science and engineering at Zhengzhou University, Zhengzhou, China. Her research interests include battery health management and reliability engineering.



Shuaijie Chen received a BS degree in Internet of Things engineering from Shenyang Ligong University, Shenyang, China, in 2022. He is currently pursuing an MS degree in engineering management at Zhengzhou University, Zhengzhou, China. His research interests include machine learning and robotic arm application technology.



Zhiqiang Cai (M'11) received a BS degree in aircraft design and engineering, an MS degree in management science and engineering, and the PhD degree in management science and engineering from Northwestern Polytechnical University (NPU), Xi'an, China, in 2003, 2006, and 2010, respectively. He is currently a Professor of Industrial Engineering with the School of Mechanical Engineering, NPU. He has authored or coauthored more than 30 academic papers and articles in journals and conferences in the past five years. His research interests include reliability modeling, importance measures, maintenance management, and decision making support.



Weiyan Liu received a PhD degree from the School of Management, Xi'an Jiaotong University, Xi'an, China. He is currently a Lecturer with the School of Management, Zhengzhou University, Zhengzhou, China. His research interests include quality management and supply chain management.



Zhenggeng Ye received a BS degree in industrial engineering from Henan University of Science and Technology, Luoyang, China, in 2012, an MS degree in industrial engineering from Jilin University, Changchun, China, in 2015, and a PhD degree in industrial engineering from Northwestern Polytechnical University, Xi'an, China, in 2021. He was a Joint PhD Student with Pennsylvania State University, University Park, Pennsylvania, USA, from 2019 to 2021. He is currently an Associate Research Fellow with the School of Management, Zhengzhou University, Zhengzhou, China. His interests include manufacturing system modeling and optimization, quality and reliability modeling, machine learning, and industrial big data analytics.